



HAL
open science

Variability of magmatic and cosmogenic ^3He in Ethiopian river sands of detrital pyroxenes: Impact on denudation rate determinations

Nicolas Puchol, Pierre-Henri Blard, Raphael Pik, Bouchaib Tibari, Jérôme Lavé

► To cite this version:

Nicolas Puchol, Pierre-Henri Blard, Raphael Pik, Bouchaib Tibari, Jérôme Lavé. Variability of magmatic and cosmogenic ^3He in Ethiopian river sands of detrital pyroxenes: Impact on denudation rate determinations. *Chemical Geology*, 2017, 448, pp.13-25. 10.1016/j.chemgeo.2016.10.033 . hal-02397079

HAL Id: hal-02397079

<https://hal.science/hal-02397079>

Submitted on 6 Sep 2020

HAL is a multi-disciplinary open access archive for the deposit and dissemination of scientific research documents, whether they are published or not. The documents may come from teaching and research institutions in France or abroad, or from public or private research centers.

L'archive ouverte pluridisciplinaire **HAL**, est destinée au dépôt et à la diffusion de documents scientifiques de niveau recherche, publiés ou non, émanant des établissements d'enseignement et de recherche français ou étrangers, des laboratoires publics ou privés.



Variability of magmatic and cosmogenic ^3He in Ethiopian river sands of detrital pyroxenes: Impact on denudation rate determinations

Nicolas Puchol, Pierre-Henri Blard ^{*}, Raphaël Pik, Bouchaïb Tibari, Jérôme Lavé

CRPG, CNRS - Université de Lorraine, UMR7358, 15 rue Notre Dame des Pauvres, 54501 Vandoeuvre-lès-Nancy, France

ARTICLE INFO

Article history:

Received 4 February 2016

Received in revised form 16 October 2016

Accepted 26 October 2016

Available online 29 October 2016

Keywords:

Ethiopia

Erosion

River sand

Cosmogenic ^3He

Magmatic correction

ABSTRACT

In-situ cosmogenic ^3He is a robust tool for determining denudation rates or exposure ages of lavas bearing mafic phenocrysts. However, analyses are often complicated by the presence of several helium sources. In particular, in old magmatic rocks with high radiogenic ^4He contents, discriminating cosmogenic ^3He from magmatic ^3He is not straightforward since these varieties may vary largely between aliquots.

We sampled sands from the Tekeze and Mile rivers, both draining the basaltic Ethiopian highlands, an area where erosion patterns are intimately linked to the development of the Western Afar margin and to heterogeneous monsoon precipitation. From each river we analyzed ~15 aliquots of pyroxenes having variable grain sizes (0.3 mm up to >1 mm). The total ^3He is both higher and more scattered in the bigger grains. Crushing of these largest grains and subsequent melting of the powder tends to produce more homogeneous ^3He values, suggesting that magmatic ^3He hosted in inclusions is responsible for most of the inter-aliquot variability. We also performed a Monte Carlo simulation based on a numerical denudation model of the two watersheds. The simulation confirms that cosmogenic ^3He variability cannot be responsible for the observed scatter since the cosmogenic ^3He variability is averaged away and unobservable in aliquots of ~200 grains. A compilation of previously published data also indicates that magmatic helium can be significantly variable, even between pre-crushed aliquots. Hence, magmatic helium, unlike cosmogenic ^3He , is highly variable, even in the case of aliquots of hundreds of grains. We suggest this is due to a strong nugget effect, possibly due to large fluid (or melt)-inclusions contained in phenocrysts.

In addition, the fact that small and big grains have comparable radiogenic ^4He concentrations suggests that grain fragmentation during river transport is responsible for the lower magmatic helium content of the smallest grains. Therefore, one should preferably use small grain (0.2–0.5 mm) granulometry for in-situ cosmogenic ^3He analysis in mafic phenocrysts.

Using the measured cosmogenic ^3He , we calculate basin-averaged denudation rates of 70 ± 20 and 57 ± 5 mm kyr⁻¹, for the Mile and for the Tekeze river, respectively. These values are coherent with long-term denudation rates previously proposed from low-temperature thermochronology.

© 2016 Elsevier B.V. All rights reserved.

1. Introduction

In-situ cosmogenic nuclides are produced by the flux of secondary cosmic particles in the top few meters of the Earth's surface. They represent a useful tool with which to quantify many key Earth-surface processes (Gosse and Phillips, 2001) for history and review. Along with other cosmogenic nuclides (e.g. ^{10}Be , ^{26}Al , ^{36}Cl , ^{21}Ne), ^3He has been widely used for the past 25 years to date lava flows (e.g. Ammon et al., 2009; Kurz et al., 1990), to reconstruct continental paleoclimates (e.g. Blard et al., 2007; Licciardi et al., 2001) or to measure in-situ (e.g. Sarda et al., 1993) or basin-averaged (e.g. Gayer et al., 2008) denudation rates. ^3He presents several advantages compared to more commonly

used isotopes like ^{10}Be or ^{26}Al . It requires neither a complex chemical preparation nor the use of an Accelerator Mass Spectrometer (AMS). Furthermore, many rocks - especially basalts - do not contain significant amounts of quartz, the mineral in which ^{10}Be and ^{26}Al are preferentially analyzed.

However, ^3He is not retained in many minerals (Trull et al., 1995). Most studies using ^3He have hence been carried out on mafic phenocrysts such as olivine and pyroxene (e.g. Kurz, 1986b), which are known to have a high helium retentivity (Blard and Pik, 2008; Shuster et al., 2004; Trull et al., 1991). In these minerals, the helium budget is a four-component system (Blard and Farley, 2008; Farley et al., 2006) consisting of:

- Cosmogenic ^3He ($^3\text{He}_c$), matrix-sited.
- Magmatic inherited ^3He and ^4He (He_{mag}), fluid (or melt) inclusion

^{*} Corresponding author.

E-mail address: blard@crpg.cnrs-nancy.fr (P.-H. Blard).

and (a small fraction) matrix-sited.

- Radiogenic ^4He ($^4\text{He}_r$), produced by the decay of ^{238}U , ^{235}U and ^{232}Th , matrix-sited.
- Nucleogenic ^3He ($^3\text{He}_{\text{nuc}}$), produced by neutron capture on Li nuclei and subsequent disintegration, matrix-sited.

For most young ($\ll 1$ Ma) mafic rocks with low U, Th and Li contents (< 10 ppm), the radiogenic and nucleogenic components can be neglected or corrected for (Blard and Farley, 2008). In this case, the cosmogenic component can be determined by a standard two-step procedure (Kurz, 1986a):

1. In vacuo mineral crushing to preferentially release and analyze inclusion-sited magmatic helium, allowing the magmatic $^3\text{He}/^4\text{He}$ ratio to be measured and also reducing the He_{mag} concentration of the residue.
2. Fusion of the same aliquot as for the crush analysis or a different aliquot of the same sample, in order to measure the bulk $(^3\text{He}/^4\text{He})_{\text{melt}}$ ratio and the total ^4He .

Then, assuming $^4\text{He}_r \sim 0$ at g^{-1} :

$$^3\text{He}_c = ^4\text{He}_{\text{melt}} \times \left[(^3\text{He}/^4\text{He})_{\text{melt}} - (^3\text{He}/^4\text{He})_{\text{mag}} \right] \quad (1)$$

Under certain conditions, one can also construct isochrons in $^3\text{He}/^4\text{He}$ vs $1/[^4\text{He}]$ space (Blard and Pik, 2008; Cerling and Craig, 1994b), thereby avoiding the first crushing step, which may trigger possible loss of matrix sited helium (Blard et al., 2006; Hilton et al., 1993; Scarsi, 2000; Yokochi et al., 2005), or, more probably, contamination by atmospheric helium (Protin et al., 2016).

However, given the concentrations of U and Th in olivine, pyroxene and in the lava matrix, the radiogenic ^4He component can rarely be neglected (Blard and Farley, 2008). Consequently, in several situations, the amount of ^4He extracted by melting the samples cannot be used to correct for the magmatic ^3He . In such cases, $^3\text{He}_c$ determinations thus require a crushing step that is sufficiently long to release and purge most of the trapped magmatic helium. If the matrix-sited magmatic helium is negligible, there is thus no more need for a magmatic helium correction. This crushing should however not be too intense in order to avoid releasing the matrix sited cosmogenic ^3He (Blard et al., 2006, 2008; Scarsi, 2000; Yokochi et al., 2005), nor contaminate the sample with atmospheric helium (Protin et al., 2016). Alternatively, a previous study (Williams et al., 2005) conducted on pyroxene microphenocrysts of Pliocene basalts of Gran Canaria (Canary Islands) has shown that the magmatic component may be negligible in the smallest grains (i.e. 125–250 μm). In the case of moderate to high (> 0.5 mm yr^{-1}) erosion rates, the cosmogenic ^3He concentration in river sands is low ($< 10^{-18}$ mol g^{-1} for watersheds with average elevation lower than 2000 m), implying that the resulting magmatic ^3He correction could represent a significant source of uncertainty. Consequently, it is important to overcome this methodological limitation, particularly for old phenocrysts that may also have significant amounts of radiogenic ^4He .

In the present study, we test the possibility of obtaining reliable cosmogenic ^3He -based denudation rates in basins dominated by old lavas. We observe that coarse-grained aliquots display very variable ^3He concentrations. However, fine-grained aliquots exhibit ^3He concentrations homogeneous enough to allow correction of the magmatic component with reasonable precision and confidence. We then examine the main cause of the variability of the coarse aliquots.

Our experiments were carried out on detrital pyroxenes from two Ethiopian rivers draining two different watersheds of the Ethiopian plateau. This work represents an important step for the study of the geomorphologic processes involved in this region, and, more generally, for estimating erosion rates in old volcanic provinces.

2. Geomorphological setting of the Ethiopian plateau and sampling

The Northwestern Ethiopian plateau is a major feature of the Ethiopian traps, a 1.5 km-thick continental flood basalt (CFB) sequence (Fig. 1) (Mohr, 1983). This imposing volcanic pile erupted 30 Ma ago, and the entire volume of basalt was emplaced in < 2 Myr (Hofmann et al., 1997; Rochette et al., 1998). On its eastern margin, along the major Afar escarpment, most of this volcanic sequence consists of ankaramitic porphyritic basalts, with local presence of ignimbrites at the top of the eruptive sequence (Ayalew et al., 2002; Pik et al., 1998, 1999). These geological characteristics are particularly well suited for ^3He analyses because rivers draining the Ethiopian plateau bear large amounts of pyroxene and olivine phenocrysts.

Determining the spatial variability of denudation rates is of great interest for understanding climate-tectonic-erosion interactions. First, erosion has a major long term influence on the global atmospheric CO_2 budget (Berner et al., 1983; Galy et al., 2007), even erosion of spatially and temporally discrete large volcanic provinces emplaced on continents (Dessert et al., 2001). Second, the development of the radial drainage network on the Ethiopian plateau is critically linked to the uplift and tectonic evolution of the plateau and its margins (Cox, 1989; McDougall et al., 1975; Pik, 2011; Pik et al., 2003; Stab et al., 2016). In this study, we focused on the comparison of two river catchments, located on both sides of the main plateau drainage divide (Fig. 1).

On the eastern side of the divide, the topographic scarp undergoes both an active morphological evolution linked to the development of its marginal graben system (Stab et al., 2016) and moderate monsoonal precipitations (700–1000 mm yr^{-1}) (Conway, 2000). The Mile river, whose watershed covers ~ 1600 km^2 with a mean slope of 13° , flows toward the Afar depression through this major topographic feature (Fig. 1). A ~ 2 kg sample of Mile river sand was collected on the 25th of February 2009, at the outlet of the basin catchment (11.62696°N ; 39.97236°E) where it reaches the Afar plain.

By contrast, the northern part of the plateau is generally lower in elevation because most of the original highland morphology has already been eroded by propagation of the Tekeze river (Fig. 1B). The upper part of the actively propagating Tekeze river catchment has a total surface of ~ 750 km^2 and a mean slope of 16° . As for the Mile river sand sample, a ~ 2 kg sample of Tekeze river sand was collected at (11.91338°N ; 38.97681°E) in February 2009. In each river, the sampled stream-bed sands are mainly composed of gravels resulting from the erosion of lavas (essentially basalts, with minor occurrence of rhyolite clasts) up to ~ 2 cm in size, single mineral grains (pyroxene, olivine and quartz), and organic debris.

It must be noted that, despite their similar mean slopes, these two watersheds display very different morphologies. While the upper part of the Tekeze river is mainly a high plateau incised by deep valleys, the Mile river hillslopes range from steep at its headwater to gentle slopes along several large North-South oriented valleys (Fig. 1B).

Cosmogenic nuclide measurement in river sands has proven to be a particularly robust method to constrain basin-averaged denudation rates at timescales of several hundreds to thousands of years (e.g. Brown et al., 1995; von Blanckenburg, 2005), while thermochronological methods quantify denudation over million year timescales (e.g. Pik et al., 2003). The two watersheds presented here are particularly well suited for cosmogenic nuclide studies because they are characterized by a homogeneous lithology, sparse vegetal cover, no ice or snow cover, limited influence of catastrophic erosive events and no significant storage of sediments (Pik et al., 1998).

3. Methods

3.1. Mineral separation

Bulk sands were sieved under flowing water into two granulometric fractions: 0.3–0.5 mm and > 0.5 mm.

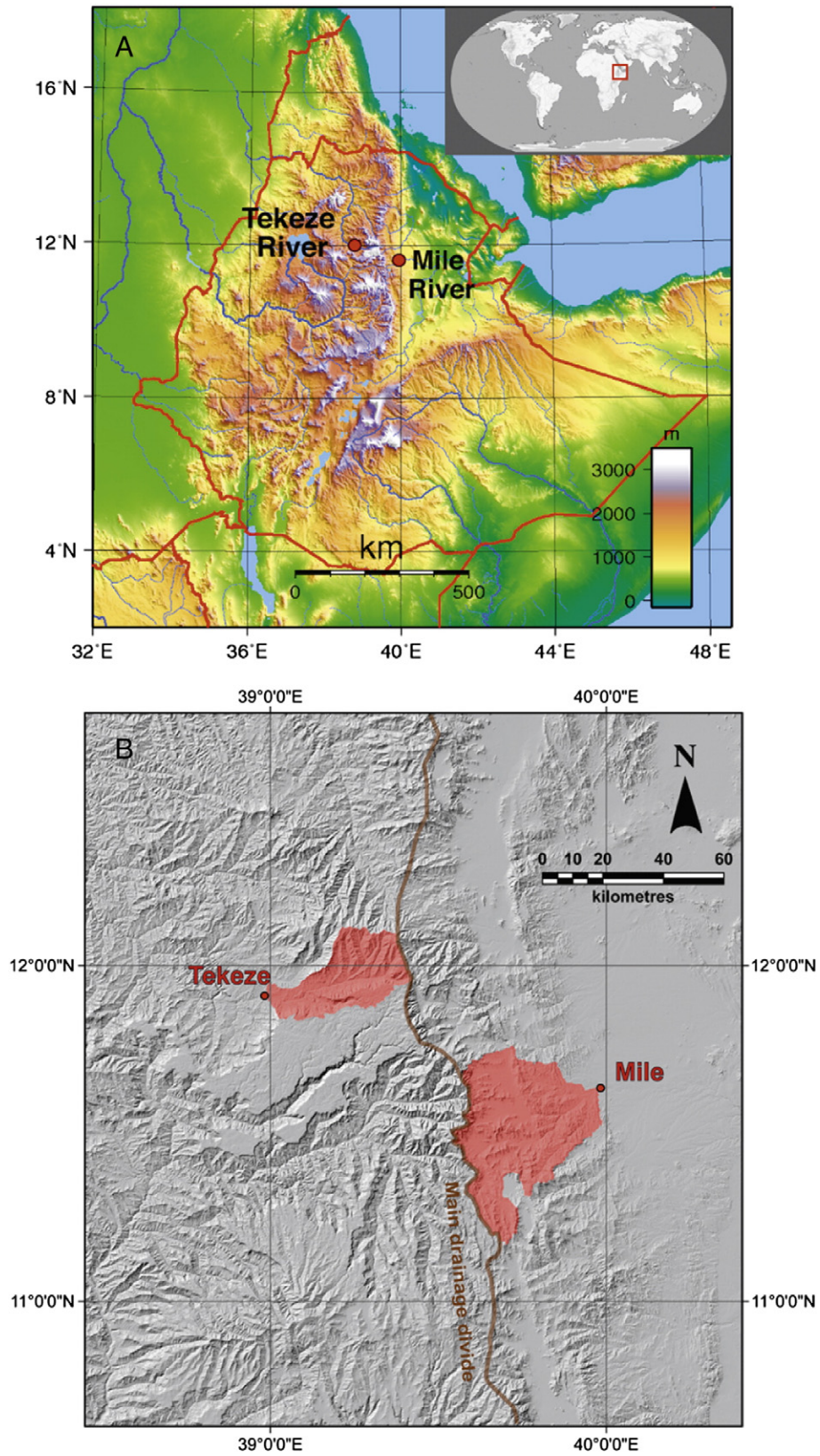


Fig. 1. Geographic situation of the studied Ethiopian rivers. A) Relief map of Ethiopia with localization of the two rivers. The WGS 84 coordinates for the sampling spots are: Tekeze River: 11.91338°N; 38.97681°E. Mile River: 11.62696°N; 39.97236°E. B) Shaded SRTM Digital Elevation Model of the study area (90 m resolution) with the two watersheds (red shadow) and their outlets (i.e. the two sampling spots, in red). The main drainage divide of the Ethiopian plateaus (brown line) follows the tectonic scarp, with rivers running toward the Blue Nile and Tekeze River in the west, and toward the Afar in the east.

Concerning the 0.3–0.5 mm fraction, pyroxene grains were first concentrated from the bulk sand by two magnetic separations using a Frantz device. Nearly pure pyroxene and olivine grains were then obtained by gravimetric separation in di-iodomethane (density $\sim 3.3 \text{ g cm}^{-3}$). After washing in diethyl ether and drying, the grains were cleaned in an ultrasonic bath of deionized water and acetone for 15 min to remove any impurities resulting from dust.

After drying, all grains with attached lava fragments were removed and discarded by handpicking under a binocular microscope. Olivine grains ($\sim 5\%$ of the phenocrysts) were also separated and set aside. We chose to work on pyroxenes because they were more abundant in our samples and thus easier to separate. We interpret these higher modal pyroxene abundances with respect to the basaltic source rocks as due to preferential abrasion and weathering of the olivines on the slopes and in the riverbed.

For the $>0.5 \text{ mm}$ fraction, phenocrysts were directly handpicked under a binocular microscope from the bulk sieved sand. They were then cleaned in a deionized water and acetone bath for 15 min.

For the Tekeze River, the $>0.5 \text{ mm}$ bulk sand remaining after the first handpicking was sieved again at 1 mm, and phenocrysts from this $>1 \text{ mm}$ bulk sand were handpicked and cleaned following the same procedure.

3.2. Analytical procedures

In-vacuo crushing extractions were performed with a soft iron slug activated by external solenoids, for 5 min at 100 strokes/min, except for one sample (Tekeze 15; 10 min). Aliquot weights ranged between 130 and 360 mg, representing ~ 100 – 300 grains for the $>0.5 \text{ mm}$ fraction and ~ 800 – 2200 grains for the 0.3–0.5 mm fraction. Typical ^4He and ^3He blanks for the crushing experiments were $(3.1 \pm 0.4) \times 10^{-16} \text{ mol}$ and $(6.0 \pm 1.4) \times 10^{-20} \text{ mol}$ respectively.

The resulting powders were then sieved to remove the $<70 \mu\text{m}$ fraction, and hence avoid grains possibly affected by loss of matrix sited helium that could have occurred during the crushing procedure (Blard et al., 2008) and limit the atmospheric contamination (Protin et al., 2016). The remaining powders and uncrushed pyroxene aliquots were subsequently wrapped in copper foils and fused at high temperature.

High temperature extractions were performed in a new high temperature furnace designed at CRPG (Nancy, France) (Zimmermann et al., 2012). After a 20-min temperature ramp, samples were maintained at $1350 \text{ }^\circ\text{C}$ for 20 min. Typical ^4He and ^3He blanks for this procedure were $(3.0 \pm 0.5) \times 10^{-18} \text{ mol}$ and $(1.1 \pm 0.8) \times 10^{-20} \text{ mol}$, respectively. Repeated extractions always yielded He contents in the blank range, indicating that the extraction was complete after the first heating step. After extraction, the gas was purified using activated charcoal at $-196 \text{ }^\circ\text{C}$ and with hot ($400 \text{ }^\circ\text{C}$ and $600 \text{ }^\circ\text{C}$) and ambient temperature ($21 \text{ }^\circ\text{C}$) Titanium sponge getters. A complete description of the furnace and the purification line can be found in Zimmermann et al. (2012).

Helium was analyzed on the GV HELIX Split Flight Tube dual collector mass spectrometer. The instrument sensitivity was determined using the HESJ standard (Matsuda et al., 2002) whose certified $^3\text{He}/^4\text{He}$ ratio is $20.63 \pm 0.10 R_a$ ($R_a = 1.384 \times 10^{-6}$ being the atmospheric $^3\text{He}/^4\text{He}$ ratio). To test the linearity of the mass spectrometer sensitivity, variable amounts of ^4He standard were analyzed: between 5×10^{-14} and $2 \times 10^{-12} \text{ mol}$.

Most of the Mile river samples were analyzed first. During a 2 month period, external reproducibility (1 σ standard deviation of sensitivity) was 2.7% and 3.9% for ^4He and ^3He , respectively.

The remaining Mile samples (the crushed Mile 5, 11, 12 and 14) and the Tekeze samples were analyzed with different ionization source settings. Over this one-month period, external reproducibility was always $<1\%$ for both ^4He and ^3He .

4. Results

All helium results are reported in Table 1 and ^3He results plotted in Fig. 2.

4.1. Crushing experiments

For the Mile river, crushing of the $>0.5 \text{ mm}$ grains yielded ^3He concentrations ranging between $(2.51 \pm 0.33) \times 10^{-18} \text{ mol g}^{-1}$ and $(5.25 \pm 0.63) \times 10^{-18} \text{ mol g}^{-1}$. $^3\text{He}/^4\text{He}$ ratios ranged between (2.73 ± 0.46) and $5.20 \pm 0.83 R_a$. One 0.3–0.5 mm sample yielded a ^3He concentration of $(2.08 \pm 0.27) \times 10^{-18} \text{ mol g}^{-1}$ with a $^3\text{He}/^4\text{He}$ ratio of $2.67 \pm 0.45 R_a$.

For the Tekeze river, crushing of the coarser grains ($>0.5 \text{ mm}$ and $>1 \text{ mm}$) yielded ^3He concentrations between $(4.20 \pm 0.12) \times 10^{-18} \text{ mol g}^{-1}$ and $(19.2 \pm 0.41) \times 10^{-18} \text{ mol g}^{-1}$, which is significantly higher than for the Mile river. This difference is probably due to differences in the petrography of the outcropping basalts in the two basins and to a longer sediment transport (see discussion in Sections 5.2 and 5.3). One 0.3–0.5 mm sample was also crushed and gave a ^3He concentration, $(2.97 \pm 0.17) \times 10^{-18} \text{ mol g}^{-1}$, lower than the range of the larger grains. $^3\text{He}/^4\text{He}$ ratios ranged between (3.39 ± 0.19) and $(13.6 \pm 0.7) R_a$.

The $^3\text{He}/^4\text{He}$ ratios measured by crushing the $>0.5 \text{ mm}$ samples of the Tekeze river are compatible with the mantle plume $^3\text{He}/^4\text{He}$ values from crushing similar high-Ti lava phenocrysts (Marty et al., 1996; Pik et al., 1999). The sampled crushed by 1000 strokes instead of only 500 is within the range of the other samples, for both ^3He concentrations and $^3\text{He}/^4\text{He}$ ratios. A five minute crushing in our apparatus seems therefore sufficient to release at least 90% of the trapped magmatic helium, as shown by Scarsi (2000) with a similar apparatus.

4.2. Heating experiments

To estimate the total amount of ^3He contained in the large grains of the Mile river ($>0.5 \text{ mm}$), either we performed a direct melting of uncrushed $>0.5 \text{ mm}$ pyroxenes (Fig. 2A), or we added the concentrations measured in the crushing and the subsequent melting steps. These experiments yield high and variable values of ^3He ($(7.35 \pm 0.31) \times 10^{-18}$ to $(15.4 \pm 2.2) \times 10^{-18} \text{ mol g}^{-1}$). Conversely, fusion of the bulk 0.3–0.5 mm grains and fusion of the powder obtained from the $>0.5 \text{ mm}$ crushed grains, yielded rather consistent and lower ^3He concentrations ($(4.62 \pm 0.39) \times 10^{-18}$ to $(6.8 \pm 1.4) \times 10^{-18} \text{ mol g}^{-1}$).

The Tekeze river samples display comparable results (Fig. 2B): small and crushed phenocrysts have lower and moderately variable ^3He concentrations ($(10.5 \pm 0.2) \times 10^{-18}$ to $(14.0 \pm 0.3) \times 10^{-18} \text{ mol g}^{-1}$), while the larger phenocrysts contain higher and more variable ^3He ($(7.18 \pm 0.18) \times 10^{-18}$ to $(24.7 \pm 0.8) \times 10^{-18}$). However, 4 out of the 12 aliquots for the $>0.5 \text{ mm}$ fraction contained less ^3He than the 0.3–0.5 mm ones. Additionally, for 6 aliquots, melting of the crushed grains of the >0.5 and $>1 \text{ mm}$ fraction yielded less ^3He than the direct melting of 0.3–0.5 mm grains, unlike the observation for the Mile River.

For all heating experiments, the $^3\text{He}/^4\text{He}$ ratios were low (between 0.29 ± 0.04 and $1.57 \pm 0.08 R_a$) for both the bulk samples and the powders (between 0.36 ± 0.02 and $0.76 \pm 0.04 R_a$). These very radiogenic values were expected, given the age of the Oligocene traps and their U-Th concentrations (Marty et al., 1996): ^4He concentrations were always $>6 \times 10^{-12} \text{ mol g}^{-1}$ in the powders.

For both river sands, crushing and heating experiments hence show that:

- The total ^3He content is on average higher in the $>0.5 \text{ mm}$ fraction (Mile river: $(10.2 \pm 2.6) \times 10^{-18} \text{ mol g}^{-1}$; Tekeze river: $(15.5 \pm 6.3) \times 10^{-18} \text{ mol g}^{-1}$) than in the 0.3–0.5 mm fraction (Mile river: $(5.48 \pm 0.40) \times 10^{-18} \text{ mol g}^{-1}$; Tekeze river: $(11.5 \pm 1.5) \times 10^{-18} \text{ mol g}^{-1}$).
- The coarse grains ($>0.5 \text{ mm}$) display more variable helium contents.

Table 1

Helium data from detrital phenocrysts of Ethiopian rivers.

Treatments: d. m. stands for “direct melting” of the phenocrysts, cr. for “crushing” and m. for “melting” of the powder obtained by crushing.

* Tekeze 15 was crushed with ~1000 strokes, instead of ~500.

 $^3\text{He}/^4\text{He}$ ratios are normalized to the atmospheric ratio $R_a = 1.384 \times 10^{-6}$.Errors are $\pm 1\sigma$.

Sample provenance and grain size	n°	Treatment	Sample mass (mg)	^3He (10^{-18} mol g $^{-1}$)	\pm	^4He (10^{-12} mol g $^{-1}$)	\pm	$^3\text{He}/^4\text{He}$ (R_a)	\pm	
Mile River 0.3–0.5 mm	1	Direct melt.	239	5.55	0.36	11.769	0.005	0.34	0.02	
	2	d. m.	250.6	5.20	0.73	12.817	0.001	0.29	0.04	
	3	d. m.	251.5	5.40	0.23	12.108	0.004	0.32	0.01	
	4	d. m.	242.9	5.79	0.69	13.20	1.38	0.32	0.05	
	5	Crushing	181.2	2.08	0.27	0.56	0.06	2.67	0.45	
		Melting	120.8	4.15	0.32	8.261	0.003	0.36	0.03	
	>0.5 mm	6	d. m.	302	12.41	0.38	–	–	–	–
		7	d. m.	141.8	8.03	0.93	9.16	0.96	0.63	0.10
		8	d. m.	158.9	9.5	1.1	8.69	0.91	0.79	0.13
		9	d. m.	171.2	15.4	2.2	9.77	1.02	1.14	0.20
		10	d. m.	260	7.35	0.31	8.670	0.001	0.61	0.17
		11	cr.	266.4	2.51	0.33	0.67	0.07	2.73	0.46
			m.		6.21	0.40	6.930	0.002	0.65	0.04
		12	cr.	237.6	5.00	0.59	0.83	0.09	4.36	0.69
		m.	101.5	4.62	0.39	6.694	0.003	0.50	0.04	
13		cr.	268.5	5.25	0.63	0.73	0.08	5.20	0.83	
	m.	166.4	6.83	1.41	6.78	0.71	0.73	0.17		
	14	cr.	162.2	4.07	0.54	0.60	0.06	4.90	0.83	
		m.	113.9	4.03	0.22	8.046	0.002	0.36	0.02	
Tekeze River 0.3–0.5 mm	1	d. m.	267.1	11.58	0.17	10.77	0.04	0.78	0.04	
	2	d. m.	232.5	10.51	0.18	12.92	0.05	0.59	0.03	
	3	d. m.	186.6	10.77	0.26	10.96	0.04	0.71	0.04	
	4	d. m.	189.5	14.02	0.28	11.17	0.04	0.91	0.05	
	5	d. m.	174.9	10.48	0.25	10.63	0.04	0.71	0.04	
	6	cr.	129	2.97	0.17	0.540	0.004	3.96	0.31	
		m.	95.1	–	–	–	–	–	–	
	>0.5 mm	7	d. m.	185.5	9.73	0.21	10.05	0.04	0.70	0.04
		8	d. m.	185.2	7.18	0.18	9.00	0.37	0.58	0.04
		9	d. m.	214	10.62	0.20	9.77	0.04	0.78	0.04
		10	d. m.	167.9	8.20	0.21	10.77	0.04	0.55	0.03
		11	d. m.	213.1	24.14	0.33	11.11	0.08	1.57	0.08
		12	cr.	330	5.61	0.10	0.378	0.002	10.71	0.58
			m.	256.5	8.69	0.17	8.30	0.03	0.76	0.04
		13	cr.	302.8	5.29	0.11	1.127	0.005	3.39	0.19
			m.	213.4	17.20	0.30	17.21	0.07	0.72	0.04
		14	cr.	380	6.54	0.14	0.853	0.004	5.53	0.31
		m.	306.8	8.98	0.19	11.56	0.05	0.56	0.03	
		15	cr.*	317.1	4.20	0.12	0.494	0.006	6.14	0.19
		m.	108.8	7.62	0.29	8.44	0.09	0.65	0.03	
	16	cr.	212.4	16.26	0.24	0.861	0.004	13.6	0.7	
	17	m.	248.7	7.82	0.18	8.84	0.04	0.64	0.04	
>1 mm	18	cr.	358.5	8.60	0.20	0.695	0.008	8.95	0.23	
		m.	65.1	6.13	0.23	9.11	0.09	0.49	0.02	
	19	cr.	306.2	19.20	0.41	1.21	0.01	11.5	0.3	
		m.	65.1	5.54	0.34	7.29	0.08	0.55	0.03	

While crushing of the bigger grains released variable amounts of ^3He , melting of the resulting powders yielded less variable and low ^3He concentrations (Fig. 2).

- The limited scatter in the ^3He concentrations measured by melting the powdered grains suggests that the crushing induced a rather uniform inter-aliquot distribution of the magmatic content.

In the following section we discuss these results taking into account the various helium sources and propose several hypotheses to explain such a grain size-dependent behavior.

5. Discussion

5.1. Influence of nucleogenic ^3He

The theoretical long-term nucleogenic ^3He production (see Section 1) in the studied samples was calculated following Andrews

and Kay (1982). We used the chemical contents reported in Pik et al. (1998) and Pik et al. (1999), and a Li concentration of 2 ppm in olivine and pyroxene, as measured by the Service d'Analyse des Roches et des Minéraux (S.A.R.M.) of CRPG (Nancy, France) in representative aliquots. The implantation and ejection correction (Farley et al., 2006) was negligible because the phenocryst-lava partition coefficient for Li is very close to 1 for these basalts. The so-calculated $^3\text{He}_n$ production rate is 1.1×10^{-26} mol g $^{-1}$ yr $^{-1}$, which yields a theoretical concentration of 3.3×10^{-19} mol g $^{-1}$ on average over 30 Myr. This value represents ~6% of the total ^3He measured in the sample bearing the lowest amount of matrix-sited ^3He . Thus, nucleogenic ^3He has only a minor influence on the studied samples, and it cannot itself explain the large inter-aliquot ^3He variability, nor the grain size dependency.

5.2. Influence of the spatial variability of denudation rates

Several studies have suggested that heterogeneous denudation rates within a drainage basin could induce a measurable inter-aliquot

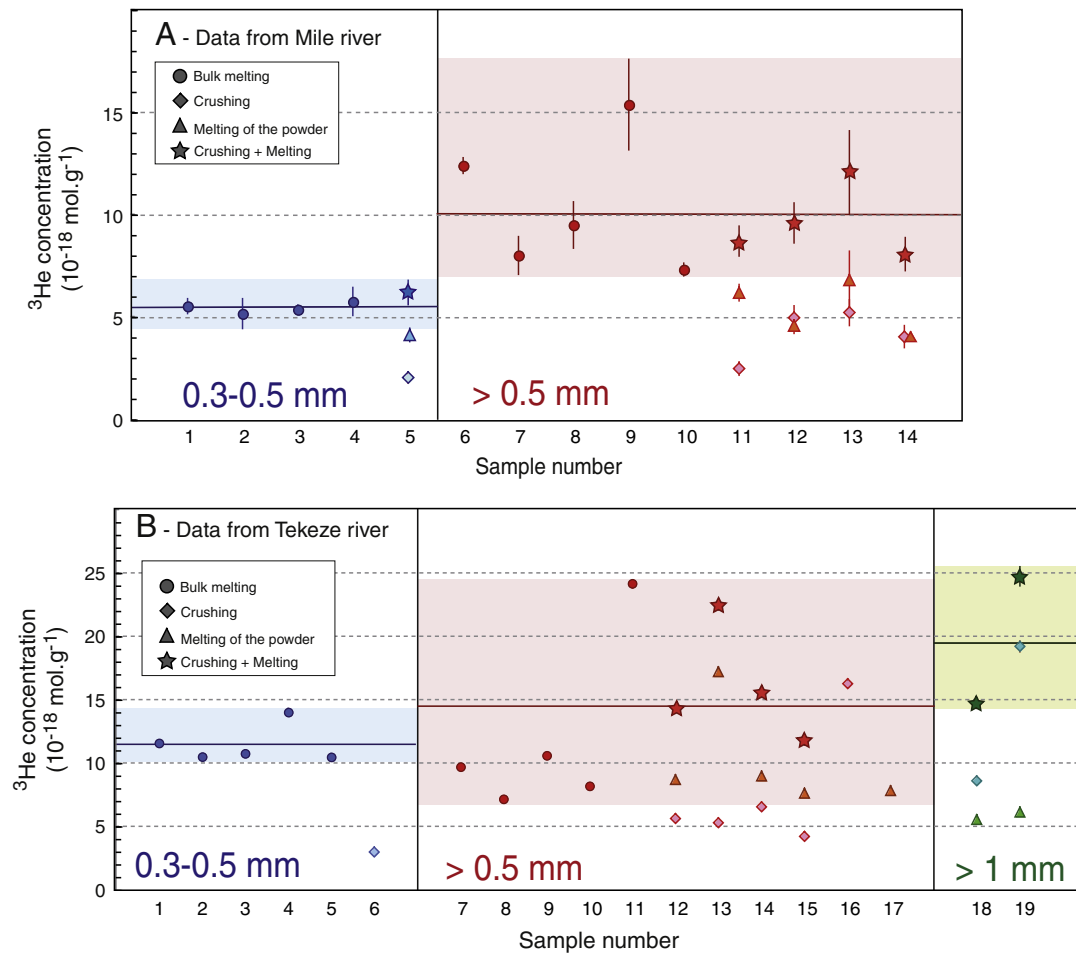


Fig. 2. Compilation of the measured ^3He concentrations in the detrital pyroxenes. A) ^3He concentrations from the Mile River sands. B) ^3He concentrations from the Tekeze River sands. Concentrations are plotted in $10^{-18} \text{ mol g}^{-1}$. The sample numbers are those used in the result table. The 0.3–0.5 mm aliquots are plotted on a blue background, the >0.5 mm ones on a red background and the >1 mm ones on a green background. For some samples, the 1σ error bars are smaller than the size of the dots. Due to analytical problems, there is no measurement for the melting of the Tekeze aliquots n°6 and 16, nor for the crushing of aliquot n°17.

variability of the cosmogenic nuclide concentration (Codilean et al., 2008; Gayer et al., 2008). Indeed, denudation rates can vary up to several orders of magnitude within the same drainage basin. Furthermore, steep drainage basins are characterized by quite variable cosmogenic nuclide production rates, because of the altitude variability (e.g. Lal, 1991; Stone, 2000).

For the two studied watersheds (Mile and Tekeze rivers), we have developed a simple Monte Carlo model to simulate the stochastic effects associated with the sampling of small aliquots of river sands. We first applied to a SRTM Digital Elevation Model (DEM) a simple fluvial shear stress incision law (Lavé and Avouac, 2001; Lavé and Burbank, 2004) from slope gradients and runoff to produce a theoretical denudation map of our watershed (Lavé, 2005). The goal of this simulation was not to produce a precise model of denudation but a realistic and first order estimate of the denudation variability within the basin. From these denudation maps, we then derived the theoretical cosmogenic nuclide concentrations at each point of the basin taking into account the local production rates. These production rates were calculated at each point of the DEM grid, using the time-independent scaling of Stone (2000), the topographic shielding of Dunne et al. (1999) and a Sea Level High Latitude production rate of $(1.99 \pm 0.16) \times 10^{-22} \text{ mol g}^{-1} \text{ yr}^{-1}$ ($120 \pm 9 \text{ at g}^{-1} \text{ yr}^{-1}$) (Goehring et al., 2010). Then, we simulated the concentration distribution of a well-mixed sand sampled at the basin outlet. Finally we randomly selected aliquots with sizes ranging from 1 to 150 grains. This simulation was performed using 500 random draws

for each aliquot size. Then, the standard deviations of these fictive aliquots were computed for each aliquot size. Results of this simulation are shown in the left part of Fig. 3.

This simulation indicates that, for both watersheds, only ~80 grains are sufficient to yield inter-aliquot standard deviation below 10% (Fig. 3). Given that the aliquots we analyzed are composed of >200 grains (standard deviation <5%), this modeling experiment with a contrived erosion scenario shows that the observed ^3He inter-aliquot variability cannot be due to stochastic sampling of grains having recorded variable denudation rates.

Consequently, the remaining most plausible cause for the observed ^3He variability between aliquots is heterogeneities in the amount of magmatic ^3He present in the different aliquots. This hypothesis is discussed in the following section.

5.3. Inter-aliquot variability: impact of the magmatic helium component

As summarized at the end of Section 4.2, crushing of the coarser aliquots released variable amounts of magmatic ^3He , while melting of the resulting powders released uniform quantities of the remaining ^3He (Fig. 2 and Table 1), most probably representing the cosmogenic component, which is sited solely in the matrix. On the other hand, melting of uncrushed pyroxenes yielded variable amounts of ^3He . These observations suggest that most of this variability is due to fluid inclusion-sited magmatic helium.

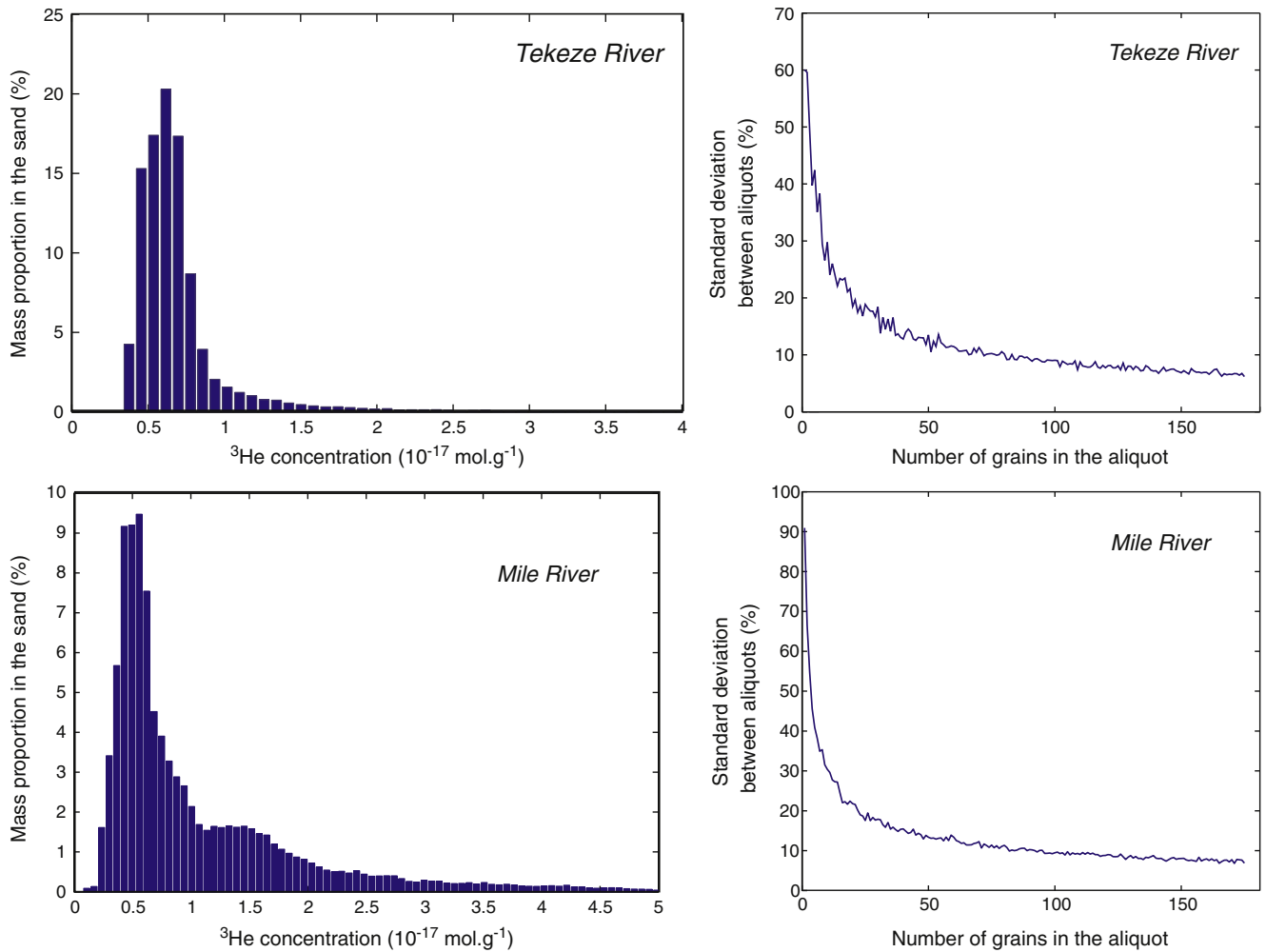


Fig. 3. Simulation of the stochastic effect of a river sand sampling at the outlet of the Mile and Tekeze rivers. Left: Distribution of cosmogenic ^3He concentrations, due to the spatial variability of denudation and production rates (300 classes were modeled here). This spatial variability was computed using an SRTM Digital Elevation Model (DEM) and a simple fluvial shear stress incision law (Lavé and Avouac, 2001; Lavé and Burbank, 2004) from slope gradient and runoff to produce a theoretical denudation map of our watershed (Lavé, 2005). These erosion rates were then converted to cosmogenic ^3He concentrations taking into account the spatial variability of production rates in the watershed (Stone, 2000). Right: Monte Carlo simulation of a stochastic sampling of the river sands. Graph shows the standard deviation of cosmogenic ^3He concentrations between 500 randomly sampled aliquots as a function of the number of grains in each aliquot.

As discussed at the end of Section 5.2, merging hundreds of grains in each aliquot is enough to homogenize the cosmogenic ^3He concentration, despite the spatial variability of the erosion of the watershed. Our data indicate that this is not necessarily the case for magmatic ^3He . In order to test this hypothesis, we summarized the magmatic ^4He concentrations measured in olivine and pyroxene phenocrysts from basalts of different geological settings (Ackert et al., 2003; Blard et al., 2006; Dunai and Wijbrans, 2000; Fenton and Niedermann, 2014; Foeken et al., 2012; Goehring et al., 2010; Kurz et al., 1990; Licciardi et al., 1999, 2006). These data combine ^4He measurements of 132 melted olivine aliquots and 32 melted pyroxene aliquots. They are presented in Table 2 and Fig. 4.

These data display mean ^4He concentrations of $5 \times 10^{-13} \text{ mol g}^{-1}$ for both olivine and pyroxene, and a significant inter-sample variability (standard deviation $> 10^{-13} \text{ mol g}^{-1}$) (Fig. 4). In these studies, lavas are young enough ($< 200 \text{ ka}$) to ensure that the radiogenic ^4He correction does not represent a significant source of uncertainty.

This compilation clearly shows that large variability in magmatic helium is common between aliquots of hundreds of grains, even when the measured aliquots originate from the same lava flow sample (Table 2). Therefore, in the case of aliquots resulting from the mixing of heterogeneous detrital material, such as in our study, it is not surprising to observe a significant variability in magmatic helium

concentrations, both for ^3He and ^4He . This nugget effect is probably larger for aliquots bearing large phenocrysts ($> 0.5 \text{ mm}$), as discussed in the following section.

5.4. Grain size dependence of the magmatic He content: insights from the radiogenic ^4He

Given the age of the basaltic sequence (30 Myr) (Hofmann et al., 1997), the crystal lattice contains large amounts of radiogenic ^4He . Most of the $^3\text{He}/^4\text{He}$ variability reported in Section 4.1 can be explained by a variable fraction of radiogenic ^4He release during the crushing, as discussed by Marty et al. (1996). The matrix-sited ^4He is furthermore known to be more prone to release during the crushing procedure than the matrix-sited cosmogenic ^3He (Scarsi, 2000).

Assuming (i) U and Th concentrations in the surrounding lava of 1.5 and 4 ppm, respectively (Pik et al., 1999), (ii) U and Th concentrations in the phenocrysts of 0.06 and 0.1 ppm, respectively (measured by ICP-MS in the samples analyzed in this study), (iii) an initial grain diameter of 3 mm, which is the size of the biggest grains found in the samples, the theoretical radiogenic ^4He concentration is $15 \times 10^{-12} \text{ mol g}^{-1}$, using the calculation of Dunai and Wijbrans (2000) (Fig. 5). This theoretical value is close to the ^4He concentrations measured by melting the phenocrysts ($(9.4 \pm 1.8) \times 10^{-12} \text{ mol g}^{-1}$ of the Mile river and $(11 \pm$

Table 2
Magmatic ^4He concentrations measured in olivine and pyroxene phenocrysts. Results are reported from various Quaternary basalts studied in previous publications (Ackert et al., 2003; Blard et al., 2006; Cerling and Craig, 1994a; Dunai and Wijbrans, 2000; Fenton and Niedermann, 2014; Foeken et al., 2012; Goehring et al., 2010; Kurz et al., 1990; Licciardi et al., 1999, 2006). These magmatic ^4He concentrations have been corrected for the radiogenic ^4He build-up (see Blard and Farley, 2008), using the U-Th concentrations in the lava and in the phenocrysts given by the original articles. When the U-Th concentrations were only measured in the lava, we used a crystal-lava partition coefficient of 0.05 (Blard and Farley, 2008). This correction is not a significant source of uncertainty.

Reference	Site	Phenocryst	Grain size (mm)	^4He (10^{-13} mol g $^{-1}$)	\pm
Fenton and Niedermann (2014)	San Francisco volcanoes, Arizona	Olivine	0.25–2	17.9	0.8
Fenton and Niedermann (2014)	San Francisco volcanoes, Arizona	Olivine	0.25–2	4.6	0.2
Fenton and Niedermann (2014)	San Francisco volcanoes, Arizona	Olivine	0.25–2	4.9	0.2
Fenton and Niedermann (2014)	San Francisco volcanoes, Arizona	Olivine	0.25–2	6.2	0.3
Fenton and Niedermann (2014)	San Francisco volcanoes, Arizona	Olivine	0.25–2	2.4	0.1
Fenton and Niedermann (2014)	San Francisco volcanoes, Arizona	Olivine	0.25–2	3.8	0.2
Fenton and Niedermann (2014)	San Francisco volcanoes, Arizona	Olivine	0.25–2	275	10
Fenton and Niedermann (2014)	San Francisco volcanoes, Arizona	Olivine	0.25–2	1.5	0.1
Fenton and Niedermann (2014)	San Francisco volcanoes, Arizona	Olivine	0.25–2	2.2	0.1
		Mean		35	
		Standard deviation		90	
Fenton and Niedermann (2014)	San Francisco volcanoes, Arizona	Pyroxene	0.25–2	1.02	0.05
Fenton and Niedermann (2014)	San Francisco volcanoes, Arizona	Pyroxene	0.25–2	3.3	0.1
Fenton and Niedermann (2014)	San Francisco volcanoes, Arizona	Pyroxene	0.25–2	1.0	0.1
Fenton and Niedermann (2014)	San Francisco volcanoes, Arizona	Pyroxene	0.25–2	2.5	0.1
Fenton and Niedermann (2014)	San Francisco volcanoes, Arizona	Pyroxene	0.25–2	1.7	0.1
Fenton and Niedermann (2014)	San Francisco volcanoes, Arizona	Pyroxene	0.25–2	1.9	0.1
Fenton and Niedermann (2014)	San Francisco volcanoes, Arizona	Pyroxene	0.25–2	5.2	0.2
Fenton and Niedermann (2014)	San Francisco volcanoes, Arizona	Pyroxene	0.25–2	87	6
Fenton and Niedermann (2014)	San Francisco volcanoes, Arizona	Pyroxene	0.25–2	25	1
Fenton and Niedermann (2014)	San Francisco volcanoes, Arizona	Pyroxene	0.25–2	2.9	0.1
Fenton and Niedermann (2014)	San Francisco volcanoes, Arizona	Pyroxene	0.25–2	0.8	0.1
		Mean		12	
		Standard deviation		26	
Ackert et al. (2003)	Patagonia volcanoes	Olivine	0.5–1	3.26	0.04
Ackert et al. (2003)	Patagonia volcanoes	Olivine	0.5–1	3.23	0.03
Ackert et al. (2003)	Patagonia volcanoes	Olivine	0.5–1	2.98	0.02
Ackert et al. (2003)	Patagonia volcanoes	Olivine	0.5–1	1.33	0.03
Ackert et al. (2003)	Patagonia volcanoes	Olivine	0.5–1	1.92	0.08
Ackert et al. (2003)	Patagonia volcanoes	Olivine	0.5–1	6.83	0.04
Ackert et al. (2003)	Patagonia volcanoes	Olivine	0.5–1	10.0	0.1
Ackert et al. (2003)	Patagonia volcanoes	Olivine	0.5–1	10.0	0.1
Ackert et al. (2003)	Patagonia volcanoes	Olivine	0.5–1	3.55	0.04
		Mean		4.8	
		Standard deviation		3.3	
Ackert et al. (2003)	Patagonia volcanoes	Pyroxene	0.5–1	1.56	0.01
Ackert et al. (2003)	Patagonia volcanoes	Pyroxene	0.5–1	1.33	0.02
Ackert et al. (2003)	Patagonia volcanoes	Pyroxene	0.5–1	1.04	0.02
Ackert et al. (2003)	Patagonia volcanoes	Pyroxene	0.5–1	1.26	0.02
		Mean		1.3	
		Standard deviation		0.2	
Licciardi et al. (1999)	Oregon volcanoes	Olivine	0.5–1	0.96	0.004
Licciardi et al. (1999)	Oregon volcanoes	Olivine	0.5–1	1.03	0.004
Licciardi et al. (1999)	Oregon volcanoes	Olivine	0.5–1	0.75	0.004
Licciardi et al. (1999)	Oregon volcanoes	Olivine	0.5–1	0.63	0.004
Licciardi et al. (1999)	Oregon volcanoes	Olivine	0.5–1	5.5	0.03
Licciardi et al. (1999)	Oregon volcanoes	Olivine	0.5–1	1.54	0.009
Licciardi et al. (1999)	Oregon volcanoes	Olivine	0.5–1	6.61	0.03
Licciardi et al. (1999)	Oregon volcanoes	Olivine	0.5–1	2.74	0.01
Licciardi et al. (1999)	Oregon volcanoes	Olivine	0.5–1	10.5	0.05
Licciardi et al. (1999)	Oregon volcanoes	Olivine	0.5–1	3.48	0.02
Licciardi et al. (1999)	Oregon volcanoes	Olivine	0.5–1	4.31	0.02
Licciardi et al. (1999)	Oregon volcanoes	Olivine	0.5–1	1.777	0.009
Licciardi et al. (1999)	Oregon volcanoes	Olivine	0.5–1	0.576	0.004
Licciardi et al. (1999)	Oregon volcanoes	Olivine	0.5–1	0.357	0.009
Licciardi et al. (1999)	Oregon volcanoes	Olivine	0.5–1	7.38	0.04
Licciardi et al. (1999)	Oregon volcanoes	Olivine	0.5–1	2.21	0.01
Licciardi et al. (1999)	Oregon volcanoes	Olivine	0.5–1	3.58	0.02
Licciardi et al. (1999)	Oregon volcanoes	Olivine	0.5–1	5.03	0.03
Licciardi et al. (1999)	Oregon volcanoes	Olivine	0.5–1	3.44	0.02
Licciardi et al. (1999)	Oregon volcanoes	Olivine	0.5–1	3.46	0.02
		Mean		3.3	
		Standard deviation		2.7	
Licciardi et al. (2006)	Iceland	Olivine	0.3–1	0.152	0.004
Licciardi et al. (2006)	Iceland	Olivine	0.3–1	0.089	0.004
Licciardi et al. (2006)	Iceland	Olivine	0.3–1	0.263	0.004
Licciardi et al. (2006)	Iceland	Olivine	0.3–1	0.049	0.004
Licciardi et al. (2006)	Iceland	Olivine	0.3–1	0.750	0.009
Licciardi et al. (2006)	Iceland	Olivine	0.3–1	0.313	0.009

Table 2 (continued)

Reference	Site	Phenocryst	Grain size (mm)	⁴ He (10 ⁻¹³ mol g ⁻¹)	±
Licciardi et al. (2006)	Iceland	Olivine	0.3–1	1.022	0.009
Licciardi et al. (2006)	Iceland	Olivine	0.3–1	0.268	0.009
Licciardi et al. (2006)	Iceland	Olivine	0.3–1	0.835	0.009
Licciardi et al. (2006)	Iceland	Olivine	0.3–1	0.393	0.009
Licciardi et al. (2006)	Iceland	Olivine	0.3–1	0.183	0.004
Licciardi et al. (2006)	Iceland	Olivine	0.3–1	0.250	0.004
Licciardi et al. (2006)	Iceland	Olivine	0.3–1	1.188	0.009
Licciardi et al. (2006)	Iceland	Olivine	0.3–1	0.036	0.004
Licciardi et al. (2006)	Iceland	Olivine	0.3–1	0.094	0.004
Licciardi et al. (2006)	Iceland	Olivine	0.3–1	0.603	0.004
Licciardi et al. (2006)	Iceland	Olivine	0.3–1	0.116	0.004
		Mean		0.4	
		Standard deviation		0.4	
Blard et al. (2006)	Etna volcano	Olivine	0.6–1	3.2	0.2
Blard et al. (2006)	Etna volcano	Olivine	0.6–1	2.0	0.1
		Mean		2.6	
		Standard deviation		0.8	
Blard et al. (2006)	Etna volcano	Pyroxene	0.6–1	0.3	0.1
Blard et al. (2006)	Etna volcano	Pyroxene	0.6–1	0.7	0.1
		Mean		0.5	
		Standard deviation		0.2	
Blard et al. (2006)	Hawaii	Olivine	0.6–1	1.0	0.1
Blard et al. (2006)	Hawaii	Olivine	0.6–1	0.5	0.1
Blard et al. (2006)	Hawaii	Olivine	0.6–1	0.7	0.1
Blard et al. (2006)	Hawaii	Olivine	0.6–1	0.32	0.04
Blard et al. (2006)	Hawaii	Olivine	0.6–1	0.0	0.1
Blard et al. (2006)	Hawaii	Olivine	0.6–1	0.2	0.1
Blard et al. (2006)	Hawaii	Olivine	0.6–1	0.9	0.1
Blard et al. (2006)	Hawaii	Olivine	0.6–1	0.08	0.03
Blard et al. (2006)	Hawaii	Olivine	0.6–1	0.1	0.1
Blard et al. (2006)	Hawaii	Olivine	0.6–1	0.7	0.1
Blard et al. (2006)	Hawaii	Olivine	0.6–1	0.3	0.1
Kurz et al. (1990)	Hawaii	Olivine	0.6–1	12.5	0.3
Kurz et al. (1990)	Hawaii	Olivine	1–2	0.3	0.01
Kurz et al. (1990)	Hawaii	Olivine	1–2	0.7	0.02
Kurz et al. (1990)	Hawaii	Olivine	1–2	2.0	0.05
Kurz et al. (1990)	Hawaii	Olivine	1–2	0.9	0.02
Kurz et al. (1990)	Hawaii	Olivine	1–2	0.3	0.01
Kurz et al. (1990)	Hawaii	Olivine	1–2	0.3	0.01
Kurz et al. (1990)	Hawaii	Olivine	1–2	0.9	0.02
Kurz et al. (1990)	Hawaii	Olivine	1–2	0.6	0.02
Kurz et al. (1990)	Hawaii	Olivine	1–2	1.1	0.03
Kurz et al. (1990)	Hawaii	Olivine	1–2	0.4	0.01
Kurz et al. (1990)	Hawaii	Olivine	1–2	6.3	0.16
Kurz et al. (1990)	Hawaii	Olivine	1–2	0.4	0.01
Kurz et al. (1990)	Hawaii	Olivine	1–2	4.1	0.10
Kurz et al. (1990)	Hawaii	Olivine	1–2	3.7	0.09
Kurz et al. (1990)	Hawaii	Olivine	1–2	10.4	0.3
Kurz et al. (1990)	Hawaii	Olivine	1–2	12.5	0.3
Kurz et al. (1990)	Hawaii	Olivine	1–2	0.40	0.01
Kurz et al. (1990)	Hawaii	Olivine	1–2	0.2	0.01
Kurz et al. (1990)	Hawaii	Olivine	1–2	0.4	0.01
Kurz et al. (1990)	Hawaii	Olivine	1–2	0.6	0.02
Kurz et al. (1990)	Hawaii	Olivine	1–2	1.9	0.05
Kurz et al. (1990)	Hawaii	Olivine	1–2	0.5	0.01
Kurz et al. (1990)	Hawaii	Olivine	1–2	2.3	0.06
Kurz et al. (1990)	Hawaii	Olivine	1–2	3.0	0.07
Kurz et al. (1990)	Hawaii	Olivine	1–2	0.2	0.00
		Mean		1.9	
		Standard deviation		3.3	
Foeken et al. (2012)	Fogo Island	Olivine	0.5–1	0.65	0.02
Foeken et al. (2012)	Fogo Island	Olivine	0.5–1	0.35	0.01
Foeken et al. (2012)	Fogo Island	Olivine	0.5–1	0.67	0.02
Foeken et al. (2012)	Fogo Island	Olivine	0.5–1	0.096	0.002
Foeken et al. (2012)	Fogo Island	Olivine	0.5–1	0.25	0.01
Foeken et al. (2012)	Fogo Island	Olivine	0.5–1	0.46	0.01
Foeken et al. (2012)	Fogo Island	Olivine	0.5–1	3.01	0.08
Foeken et al. (2012)	Fogo Island	Olivine	0.5–1	0.24	0.01
Foeken et al. (2012)	Fogo Island	Olivine	0.5–1	1.16	0.03
Foeken et al. (2012)	Fogo Island	Olivine	0.5–1	0.32	0.01
Foeken et al. (2012)	Fogo Island	Olivine	0.5–1	0.31	0.01
		Mean		0.7	
		Standard deviation		0.8	

(continued on next page)

Table 2 (continued)

Reference	Site	Phenocryst	Grain size (mm)	^4He (10^{-13} mol g $^{-1}$)	\pm
Foeken et al. (2012)	Fogo Island	Pyroxene	0.5–1	0.79	0.02
Foeken et al. (2012)	Fogo Island	Pyroxene	0.5–1	0.46	0.01
Foeken et al. (2012)	Fogo Island	Pyroxene	0.5–1	1.16	0.03
Foeken et al. (2012)	Fogo Island	Pyroxene	0.5–1	0.54	0.01
Foeken et al. (2012)	Fogo Island	Pyroxene	0.5–1	1.93	0.05
Foeken et al. (2012)	Fogo Island	Pyroxene	0.5–1	3.42	0.09
Foeken et al. (2012)	Fogo Island	Pyroxene	0.5–1	2.23	0.06
Foeken et al. (2012)	Fogo Island	Pyroxene	0.5–1	2.13	0.05
Foeken et al. (2012)	Fogo Island	Pyroxene	0.5–1	5.09	0.13
Foeken et al. (2012)	Fogo Island	Pyroxene	0.5–1	3.67	0.09
Foeken et al. (2012)	Fogo Island	Pyroxene	0.5–1	7.99	0.20
		Mean		2.7	
		Standard deviation		2.3	
Dunai and Wijbrans (2000)	Canary Island	Olivine	0.2–0.4	42.2	0.3
Dunai and Wijbrans (2000)	Canary Island	Olivine	0.2–0.4	31.1	0.2
Dunai and Wijbrans (2000)	Canary Island	Olivine	0.2–0.4	10.5	0.1
Dunai and Wijbrans (2000)	Canary Island	Olivine	0.2–0.4	35.4	0.2
Dunai and Wijbrans (2000)	Canary Island	Olivine	0.2–0.4	33.0	0.2
Dunai and Wijbrans (2000)	Canary Island	Olivine	0.2–0.4	67.1	0.5
Dunai and Wijbrans (2000)	Canary Island	Olivine	0.2–0.4	88.0	0.7
Dunai and Wijbrans (2000)	Canary Island	Olivine	0.2–0.4	27.1	0.2
Dunai and Wijbrans (2000)	Canary Island	Olivine	0.2–0.4	18.4	0.2
Dunai and Wijbrans (2000)	Canary Island	Olivine	0.2–0.4	24.9	0.2
		Mean		38	
		Standard deviation		23	
Goehring et al. (2010)	Tabernacle Hill basalt	Olivine	0.5–1	3.7	0.1
Goehring et al. (2010)	Tabernacle Hill basalt	Olivine	0.5–1	5.5	0.1
Goehring et al. (2010)	Tabernacle Hill basalt	Olivine	0.5–1	4.7	0.1
Goehring et al. (2010)	Tabernacle Hill basalt	Olivine	0.5–1	5.7	0.1
Goehring et al. (2010)	Tabernacle Hill basalt	Olivine	0.5–1	6.6	0.2
Goehring et al. (2010)	Tabernacle Hill basalt	Olivine	0.5–1	5.0	0.1
Goehring et al. (2010)	Tabernacle Hill basalt	Olivine	0.5–1	4.4	0.1
Goehring et al. (2010)	Tabernacle Hill basalt	Olivine	0.5–1	6.4	0.2
Goehring et al. (2010)	Tabernacle Hill basalt	Olivine	0.5–1	15.2	0.4
		Mean		6	
		Standard deviation		3	
Cerling and Craig (1994a, 1994b)	Western USA basalts	Olivine	0.5–1	0.48	0.01
Cerling and Craig (1994a, 1994b)	Western USA basalts	Olivine	0.5–1	0.27	0.01
Cerling and Craig (1994a, 1994b)	Western USA basalts	Olivine	0.5–1	1.34	0.03
Cerling and Craig (1994a, 1994b)	Western USA basalts	Olivine	0.5–1	2.09	0.05
Cerling and Craig (1994a, 1994b)	Western USA basalts	Olivine	0.5–1	0.64	0.02
Cerling and Craig (1994a, 1994b)	Western USA basalts	Olivine	0.5–1	0.57	0.01
Cerling and Craig (1994a, 1994b)	Western USA basalts	Olivine	0.5–1	0.19	0.00
Cerling and Craig (1994a, 1994b)	Western USA basalts	Olivine	0.5–1	0.44	0.01
		Mean		0.8	
		Standard deviation		0.6	
Cerling and Craig (1994a, 1994b)	Western USA basalts	Pyroxene	0.5–1	0.65	0.02
Cerling and Craig (1994a, 1994b)	Western USA basalts	Pyroxene	0.5–1	3.58	0.09
Cerling and Craig (1994a, 1994b)	Western USA basalts	Pyroxene	0.5–1	0.72	0.02
Cerling and Craig (1994a, 1994b)	Western USA basalts	Pyroxene	0.5–1	0.24	0.01
		Mean		1.3	
		Standard deviation		1.5	

$2) \times 10^{-12}$ mol g $^{-1}$ for the Tekeze), and is an order of magnitude higher than the average magmatic ^4He concentrations determined by crushing (Table 1).

An additional argument that all of the pyroxene grains were derived from phenocrysts of large and similar size comes from consideration of the impact of the grain size on the expected $^4\text{He}_r$ contents. The amount of implanted radiogenic ^4He theoretically increases with smaller phenocryst sizes (e.g. Dunai and Wijbrans, 2000; Blard and Farley, 2008). A 0.3 mm grain would for instance contain 27×10^{-12} mol g $^{-1}$ of $^4\text{He}_r$, and a 1 mm grain 19×10^{-12} mol g $^{-1}$, both being significantly higher than what we measured in the pyroxene grains. Therefore the fact that the ^4He concentrations are very similar between the small and big grains suggests that all phenocrysts had similar initial size (Fig. 5). This argument would however be incorrect if river transport had removed the $^4\text{He}^*$ rich external skin (typically 20 μm) by an attrition process. Nevertheless, theoretical (Jerolmack and Brzinski, 2010) and experimental studies (Kuenen, 1959) indicate that attrition (and abrasion) is not very efficient during fluvial transport of sediments.

Consequently, the present-day distribution of the phenocryst sizes observed in the river bedload most probably results from grain fragmentation during pedogenesis or sediment transport.

In addition, we observe that the vacuum crushing of the coarser grains released significantly higher amounts of ^3He than for the smaller grains. Our results also show a larger variability of the magmatic helium concentration in larger grains (Section 5.3).

Bigger minerals generally contain more magmatic helium than the smaller ones, in line with the conclusions of Williams et al. (2005). These authors proposed that the higher magmatic helium content of the bigger grains is a consequence of magmatic processes. The microphenocrysts may have crystallized at shallower depth than the larger ones, in a more degassed magma, trapping hence lower amounts of magmatic helium in their crystal lattice. Another explanation may also be that bigger phenocrysts have a higher probability of bearing large fluid inclusions. This alternative hypothesis is supported by the large inter-sample variability of magmatic helium (Fig. 4). Large nugget-effects are indeed more probably explained if magmatic helium is

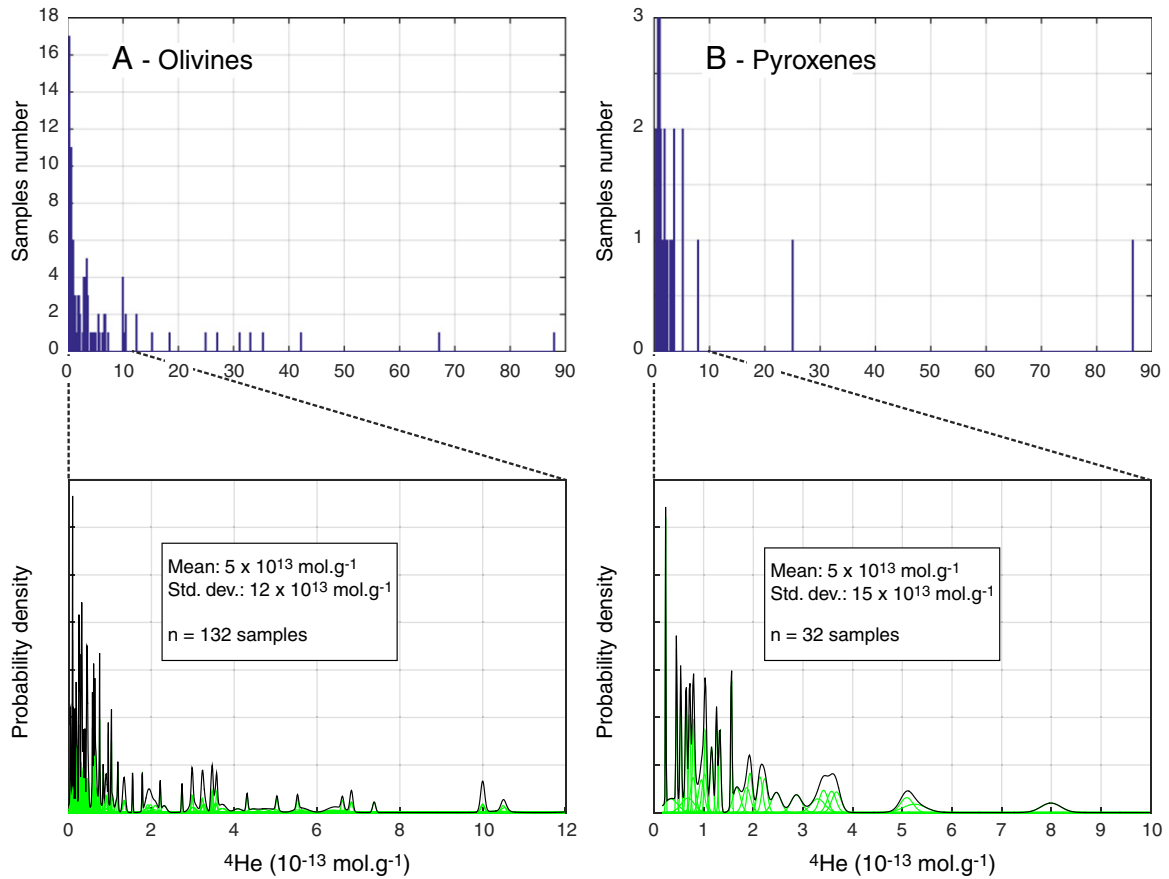


Fig. 4. Distribution of magmatic ^4He concentrations in olivine (A) and pyroxene (B) phenocrysts, compiled from various studies (Ackert et al., 2003; Blard et al., 2006; Cerling and Craig, 1994a; Dunai and Wijbrans, 2000; Fenton and Niedermann, 2014; Foeken et al., 2012; Goehring et al., 2010; Kurz et al., 1990; Licciardi et al., 1999, 2006). These data are presented in Table 2. All of these concentrations were measured by in vacuo melting of phenocrysts, ensuring a total release of the magmatic helium from the minerals. All abscissa axes are scaled in $10^{-13} \text{ mol g}^{-1}$. In all of these studies, typical aliquot sizes were between 0.1 and 1 g, ensuring the presence of hundreds to thousands of grains. This compilation clearly indicates a high variability of the concentrations in magmatic helium. These magmatic ^4He concentrations have been corrected for the radiogenic ^4He build-up (see Blard and Farley, 2008), using the U-Th concentrations in the lava and in the phenocrysts given by the original articles. When the U-Th concentrations were only measured in the lava, we used a crystal-lava partition coefficient of 0.05 (Blard and Farley, 2008). This correction is not a significant source of uncertainty.

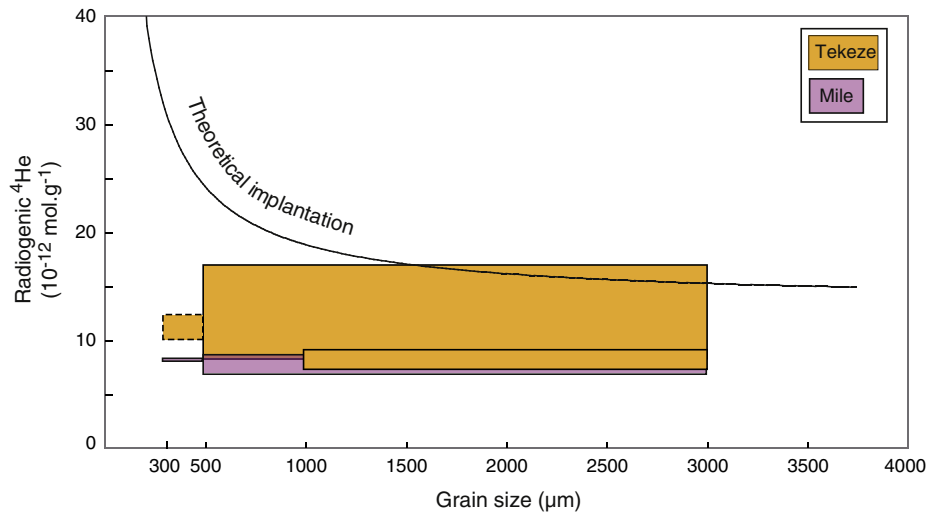


Fig. 5. Theoretical and measured radiogenic ^4He as a function of grain size. The theoretical model for α -implantation is computed from the equations of Dunai and Wijbrans (2000). Orange and purple boxes show the distribution of the measured radiogenic components ($^4\text{He}_r$) in the Tekeze and Mile river phenocrysts. $^4\text{He}_r$ is determined by melting grains that were previously crushed to remove their magmatic ^4He (Table 1). There are no similar data for the 300–500 μm fraction of the Tekeze river, so we calculated $^4\text{He}_r$ in this case by subtracting the ^4He extracted by crushing of an aliquot from the total ^4He in other bulk aliquots. Concentrations are similar in all granulometric fractions and lower than the theoretical value, which suggests that small grains result from crushing during river transport. Alternatively, a loss of a small fraction of ^4He , during in vacuo crushing is possible (see Section 5.4).

carried by fluid inclusions than by the mineral lattice. The nugget effect is limited by the maximum possible size of the nugget: the maximum inclusion size in the fine fraction is pretty small in small grains. However, a detailed comprehensive petrographic study would be necessary to confirm this interpretation. To do so, it would be useful to characterize the distribution of fluid inclusions in phenocrysts, as well as their relation with grain size.

In any case, these observations support the idea that the smaller river grains result from the crushing of bigger grains during riverbed transport and hillslope processes. This natural crushing of the phenocrysts may have released an important amount of the fluid inclusion-sited helium, reducing their magmatic ^3He content and inducing a lower inter-aliquot variability.

5.5. Denudation rates and geographic distribution over the margin and the Ethiopian plateau

Because it is not possible to simply use the magmatic $^3\text{He}/^4\text{He}$ ratio to correct such radiogenic ^4He rich Oligocene pyroxenes (Eq. (1)), the only way to calculate and derive a reasonable value for the cosmogenic ^3He concentration is to use the most accurate estimate of the magmatic ^3He concentration, and subtract it from the total ^3He . The investigation of the He budget that we have done in this study has shown that the magmatic He concentration of a sample may scatter significantly for coarse grain sizes (>0.5 mm), whereas it is lower and rather homogeneous for the smallest granulometric fraction (0.3–0.5 mm) (Table 1; Fig. 2). Therefore, we propose to perform the magmatic ^3He correction using the ^3He concentration measured by crushing aliquots having a similar grain size to that of the fraction analyzed by heating. We stress that this can only be done for the smaller grains (0.3–0.5 mm) because they have reasonably low inter-aliquot variabilities (Fig. 2; Table 1) which do not induce prohibitive error on the estimated magmatic ^3He value. Following this reasoning, we use corrections for magmatic ^3He of $(2.08 \pm 0.27) \times 10^{-18} \text{ mol g}^{-1}$ and $(2.97 \pm 0.17) \times 10^{-18} \text{ mol g}^{-1}$ for the Mile and the Tekeze river, respectively. These uncertainties include the inter-aliquot variability of the ^3He concentrations determined by crushing. This yields mass-weighted average $^3\text{He}_c$ concentrations of $(3.4 \pm 0.6) \times 10^{-18} \text{ mol g}^{-1}$ for the Mile river and $(8.5 \pm 1.5) \times 10^{-18} \text{ mol g}^{-1}$ for the Tekeze river. In both cases, this magmatic ^3He correction represents about 30% of the total ^3He extracted by fusing the 0.3–0.5 mm aliquots.

The basin-averaged denudation rate can thus be calculated applying (Brown et al., 1995; Lal, 1991):

$$\varepsilon = P \times \Lambda / (\rho \times ^3\text{He}_c) \quad (2)$$

where P is the basin-averaged surface $^3\text{He}_c$ production rate (see Section 5.3), Λ the typical attenuation length (160 g cm^{-2} , Gosse and Phillips, 2001), and ρ the density of the rock (2.7 g cm^{-3}).

The obtained average denudation rates are $70 \pm 20 \text{ mm kyr}^{-1}$ and $57 \pm 11 \text{ mm kyr}^{-1}$ for the Mile and Tekeze river watersheds, respectively. These similar values are consistent with the fact that both watersheds have comparable geology, steepness and pluviometry (Conway, 2000). Such denudation rates are also consistent with long term (the last 5–10 Myr) denudation rates ($90\text{--}180 \text{ mm kyr}^{-1}$) proposed for a similar geomorphologic and climatic setting in this region by Pik et al. (2003), based on low temperature (U-Th)/ ^4He thermochronology. The very long term (last 25–29 Myr) denudation rate of the central plateau is however lower (30 mm kyr^{-1}) than our values derived from cosmogenic nuclides (Pik et al., 2003). However in this area, the denudation is concentrated in the upper parts of the drainage system where the headwaters are quickly retreating into the plateau (Pik et al., 2003). Hence, small and upstream catchments such as those of the Tekeze and Mile rivers are expected to display higher recent denudation rates than the long term rates for the broader region.

6. Conclusions

Crushing and heating experiments conducted on the detrital sands of two Ethiopian rivers indicate that the coarser pyroxene phenocrysts (>0.5 mm) have higher and more variable concentrations in ^3He than the smaller ones (0.3–0.5 mm). Initial crushing of the coarser grains reduces most of the discrepancies in bulk ^3He concentrations obtained by subsequent melting. This suggests that magmatic ^3He is responsible for most of this variability. Also, crushing experiments show that smaller phenocrysts tend to have lower concentrations of magmatic ^3He . Moreover, Monte-Carlo simulations of sand sampling in these basins shows that, for a homogenous granulometry and a well-mixed sand, spatial variation of erosion should induce only negligible variations in cosmogenic ^3He for aliquots of several hundreds of grains. Our interpretation is that the observed inter aliquot variability results from variable concentrations of magmatic helium: large phenocrysts are more likely to contain high and variable amounts of magmatic helium. Even several hundreds of grains are not enough to homogenize these heterogeneities and avoid “nugget effects”. This may pose challenges to accurate determination of cosmogenic ^3He .

Consequently, the more suitable small fraction (0.3–0.5 mm) should be used to measure magmatic He concentrations by crushing, which can then be used to derive accurate cosmogenic ^3He concentrations.

In our case, these smaller grains are probably former bigger grains that have been broken during transport in the rivers and which have consequently lost a significant proportion of their magmatic helium. This hypothesis is supported by the homogenous radiogenic ^4He implantation found in all grain sizes.

Average cosmogenic ^3He concentrations measured in the 0.3–0.5 mm aliquots yield average denudation rates of $70 \pm 20 \text{ mm kyr}^{-1}$ for the Mile river basin and $57 \pm 11 \text{ mm kyr}^{-1}$ for the Tekeze river basin. These rates are in good agreement with long-term denudation rates of the Ethiopian plateau as estimated by low temperature thermochronology (Pik et al., 2003).

Acknowledgements

D. Ayalew and G. Yirgu are thanked for their assistance in the field in Ethiopia. This work has been partially funded by the INSU program “Relief de la Terre”. Samuel Niedermann and Ken Farley are acknowledged for their constructive and very thorough review that significantly improved the manuscript. We are particularly grateful to our colleague Laurie Reisberg who checked the English quality of the manuscript. This is CRPG contribution n°2469.

References

- Ackert, R.P., Singer, B.S., Guillou, H., Kaplan, M.R., Kurz, M.D., 2003. Long-term cosmogenic ^3He production rates from $^{40}\text{Ar}/^{39}\text{Ar}$ and K-Ar dated Patagonian lava flows at 47°S. *Earth Planet. Sci. Lett.* 210, 119–136.
- Ammon, K., Dunai, T.J., Stuart, F.M., Meriaux, A.S., Gayer, E., 2009. Cosmogenic ^3He exposure ages and geochemistry of basalts from Ascension Island, Atlantic Ocean. *Quat. Geochronol.* 4, 525–532.
- Andrews, J.N., Kay, R.L.F., 1982. Natural production of tritium in permeable rocks. *Nature* 298, 361–363.
- Ayalew, D., Barbey, P., Marty, B., Reisberg, L., Yirgu, G., Pik, R., 2002. Source, genesis, and timing of giant ignimbrite deposits associated with Ethiopian continental flood basalts. *Geochim. Cosmochim. Acta* 66, 1429–1448.
- Berner, R.A., Lasaga, A.C., Garrels, R.M., 1983. The carbonate-silicate geochemical cycle and its effect on atmospheric carbon-dioxide over the past 100 million years. *Am. J. Sci.* 283, 641–683.
- Blard, P.-H., Farley, K.A., 2008. The influence of radiogenic ^4He on cosmogenic ^3He determinations in volcanic olivine and pyroxene. *Earth Planet. Sci. Lett.* 276, 20–29.
- Blard, P.-H., Pik, R., 2008. An alternative isochron method for measuring cosmogenic ^3He in lava flows. *Chem. Geol.* 251, 20–32.
- Blard, P.-H., Pik, R., Lavé, J., Bourlès, D., Burnard, P.G., Yokochi, R., Marty, B., Trusdell, F., 2006. Cosmogenic ^3He production rates revisited from evidences of grain size dependent release of matrix sited helium. *Earth Planet. Sci. Lett.* 247, 222–234.
- Blard, P.-H., Lave, J., Pik, R., Wagnon, P., Bourles, D., 2007. Persistence of full glacial conditions in the Central Pacific until 15,000 years ago. *Nature* 449, 591–594.

- Blard, P.-H., Puchol, N., Farley, K.A., 2008. Constraints on the loss of matrix-sited helium during vacuum crushing of mafic phenocrysts. *Geochim. Cosmochim. Acta* 72, 3788–3803.
- Brown, E.T., Stallard, R.F., Larsen, M.C., Raisbeck, G.M., Yiou, F., 1995. Denudation rates determined from the accumulation of in situ produced ^{10}Be in the Luquillo experimental forest, Puerto-Rico. *Earth Planet. Sci. Lett.* 129, 193–202.
- Cerling, T.E., Craig, H., 1994a. Cosmogenic ^3He production rates from 39°N to 46°N latitude, western USA and France. *Geochim. Cosmochim. Acta* 58, 249–255.
- Cerling, T.E., Craig, H., 1994b. Geomorphology and in-situ cosmogenic isotopes. *Annu. Rev. Earth Planet. Sci.* 22, 273–317.
- Codilean, A.T., Bishop, P., Stuart, F.M., Hoey, T.B., Fabel, D., Freeman, S., 2008. Single-grain cosmogenic ^{21}Ne concentrations in fluvial sediments reveal spatially variable erosion rates. *Geology* 36, 159–162.
- Conway, D., 2000. The climate and hydrology of the Upper Blue Nile river. *Geogr. J.* 166, 49–62.
- Cox, K.G., 1989. The role of mantle plumes in the development of continental drainage patterns. *Nature* 342, 873–877.
- Dessert, C., Dupré, B., François, L.M., Schott, J., Gaillardet, J., Chakrapani, G., Bajpai, S., 2001. Erosion of Deccan traps determined by river geochemistry: impact on the global climate and the $^{87}\text{Sr}/^{86}\text{Sr}$ ratio of seawater. *Earth Planet. Sci. Lett.* 188, 459–474.
- Dunai, T.J., Wijbrans, J.R., 2000. Long-term cosmogenic ^3He production rates (152 ka–1.35 Ma) from $^{40}\text{Ar}/^{39}\text{Ar}$ dated basalt flows at 29°N latitude. *Earth Planet. Sci. Lett.* 176, 147–156.
- Dunne, J., Elmore, D., Muzikar, P., 1999. Scaling factors for the rates of production of cosmogenic nuclides for geomorphic shielding and attenuation at depth on sloped surfaces. *Geomorphology* 27, 3–11.
- Farley, K.A., Libarkin, J., Mukhopadhyay, S., Amidon, W., 2006. Cosmogenic and nucleogenic ^3He in apatite, titanite, and zircon. *Earth Planet. Sci. Lett.* 248, 451–461.
- Fenton, C.R., Niedermann, S., 2014. Surface exposure dating of young basalts (1–200 ka) in the San Francisco volcanic field (Arizona, USA) using cosmogenic ^3He and ^{21}Ne . *Quat. Geochronol.* 19, 87–105.
- Foeken, J.P.T., Stuart, F.M., Mark, D.F., 2012. Long-term low latitude cosmogenic ^3He production rate determined from a 126 ka basalt from Fogo, Cape Verdes. *Earth Planet. Sci. Lett.* 359–360, 14–25.
- Galy, V., France-Lanord, C., Beyssac, O., Faure, P., Kudrass, H., Palhol, F., 2007. Efficient organic carbon burial in the Bengal fan sustained by the Himalayan erosional system. *Nature* 450, 407–410.
- Gayer, E., Mukhopadhyay, S., Meade, B.J., 2008. Spatial variability of erosion rates inferred from the frequency distribution of cosmogenic ^3He in olivines from Hawaiian river sediments. *Earth Planet. Sci. Lett.* 266, 303–315.
- Goehring, B.M., Kurz, M.D., Balco, G., Schaefer, J.M., Licciardi, J., Lifton, N.A., 2010. A reevaluation of in situ cosmogenic ^3He production rates. *Quat. Geochronol.* 5, 410–418.
- Gosse, J.C., Phillips, F.M., 2001. Terrestrial in situ cosmogenic nuclides: theory and application. *Quat. Sci. Rev.* 20, 1475–1560.
- Hilton, D.R., Hammerschmidt, K., Teufel, S., Friedrichsen, H., 1993. Helium isotope characteristics of Andean geothermal fluids and lavas. *Earth Planet. Sci. Lett.* 120, 265–282.
- Hofmann, C., Courtillot, V., Feraud, G., Rochette, P., Yirgu, G., Ketefo, E., Pik, R., 1997. Timing of the Ethiopian flood basalt event and implications for plume birth and global change. *Nature* 389, 838–841.
- Jerolmack, D.J., Brzinski, T.A., 2010. Equivalence of abrupt grain-size transitions in alluvial rivers and eolian sand seas: a hypothesis. *Geology* 38 (8), 719–722.
- Kuenen, P.H., 1959. Experimental abrasion; 3, Fluvial action on sand. *Am. J. Sci.* 257 (3), 172–190.
- Kurz, M.D., 1986a. Cosmogenic helium in a terrestrial igneous rock. *Nature* 320, 435–439.
- Kurz, M.D., 1986b. In situ production of terrestrial cosmogenic helium and some applications to geochronology. *Geochim. Cosmochim. Acta* 50, 2855–2862.
- Kurz, M.D., Colodner, D., Trull, T.W., Moore, R.B., O'Brien, K., 1990. Cosmic-ray exposure dating with in situ produced cosmogenic ^3He - results from young Hawaiian lava flows. *Earth Planet. Sci. Lett.* 97, 177–189.
- Lal, D., 1991. Cosmic ray labeling of erosion surfaces: in situ nuclide production rates and erosion models. *Earth Planet. Sci. Lett.* 104, 424–439.
- Lavé, J., 2005. Analytic solution of the mean elevation of a watershed dominated by fluvial incision and hillslope landslides. *Geophys. Res. Lett.* 32. <http://dx.doi.org/10.1029/2005GL022482>.
- Lavé, J., Avouac, J.P., 2001. Fluvial incision and tectonic uplift across the Himalayas of Central Nepal. *J. Geophys. Res. Solid Earth* 106, 26561–26591.
- Lavé, J., Burbank, D., 2004. Denudation processes and rates in the Transverse Ranges, southern California: erosional response of a transitional landscape to external and anthropogenic forcing. *J. Geophys. Res. Earth Surf.* 109:F01006. <http://dx.doi.org/10.1029/2003JF000023>.
- Licciardi, J.M., Kurz, M.D., Clark, P.U., Brook, E.J., 1999. Calibration of cosmogenic ^3He production rates from Holocene lava flows in Oregon, USA, and effects of the Earth's magnetic field. *Earth Planet. Sci. Lett.* 172, 261–271.
- Licciardi, J.M., Clark, P.U., Brook, E.J., Pierce, K.L., Kurz, M.D., Elmore, D., Sharma, P., 2001. Cosmogenic ^3He and ^{10}Be chronologies of the late Pinedale northern Yellowstone ice cap, Montana, USA. *Geology* 29, 1095–1098.
- Licciardi, J.M., Kurz, M.D., Curtice, J.M., 2006. Cosmogenic ^3He production rates from Holocene lava flows in Iceland. *Earth Planet. Sci. Lett.* 246, 251–264.
- Marty, B., Pik, R., Gezahegn, Y., 1996. Helium isotopic variations in Ethiopian plume lavas: nature of magmatic sources and limit on lower mantle contribution. *Earth Planet. Sci. Lett.* 144, 223–237.
- Matsuda, J., Matsumoto, T., Sumino, H., Nagao, K., Yamamoto, J., Miura, Y., Kaneoka, I., Takahata, N., Sano, Y., 2002. The $^3\text{He}/^4\text{He}$ ratio of the new internal He standard of Japan (HESJ). *Geochem. J.* 36, 191–195.
- McDougall, I., Morton, W.H., Williams, M.A.J., 1975. Age and rates of denudation of trap series basalts at Blue Nile Gorge, Ethiopia. *Nature* 254, 207–209.
- Mohr, P., 1983. Ethiopian flood-basalt province. *Nature* 303, 577–584.
- Pik, R., 2011. Geodynamics: East Africa on the rise. *Nat. Geosci.* 4, 660–661.
- Pik, R., Deniel, C., Coulon, C., Yirgu, G., Hofmann, C., Ayalew, D., 1998. The northwestern Ethiopian plateau flood basalts. Classification and spatial distribution of magma types. *J. Volcanol. Geotherm. Res.* 81, 91–111.
- Pik, R., Deniel, C., Coulon, C., Yirgu, G., Marty, B., 1999. Isotopic and trace element signatures of Ethiopian flood basalts: evidence for plume-lithosphere interactions. *Geochim. Cosmochim. Acta* 63, 2263–2279.
- Pik, R., Marty, B., Carignan, J., Lavé, J., 2003. Stability of the Upper Nile drainage network (Ethiopia) deduced from (U-Th)/He thermochronometry: implications for uplift and erosion of the Afar plume dome. *Earth Planet. Sci. Lett.* 215, 73–88.
- Protin, M., Blard, P.-H., Marrocchi, Y., Mathon, F., 2016. Irreversible adsorption of atmospheric helium on olivine surfaces: a lobster pot analogy. *Geochim. Cosmochim. Acta* 179, 76–88.
- Rochette, P., Tamrat, E., Feraud, G., Pik, R., Courtillot, V., Ketefo, E., Coulon, C., Hoffmann, C., Vandamme, D., Yirgu, G., 1998. Magnetostratigraphy and timing of the Oligocene Ethiopian traps. *Earth Planet. Sci. Lett.* 164, 497–510.
- Sarda, P., Staudacher, T., Allègre, C.J., Lecomte, A., 1993. Cosmogenic neon and helium at Réunion: measurement of erosion rate. *Earth Planet. Sci. Lett.* 119, 405–417.
- Scarsi, P., 2000. Fractional extraction of helium by crushing of olivine and clinopyroxene phenocrysts: effects on the $^3\text{He}/^4\text{He}$ measured ratio. *Geochim. Cosmochim. Acta* 64, 3751–3762.
- Shuster, D.L., Farley, K.A., Sistierson, J.M., Burnett, D.S., 2004. Quantifying the diffusion kinetics and spatial distributions of radiogenic ^4He in minerals containing proton-induced ^3He . *Earth Planet. Sci. Lett.* 217, 19–32.
- Stab, M., Bellahsen, N., Pik, R., Quidelleur, X., Ayalew, D., Leroy, S., 2016. Mode of rifting in magma-rich settings: tectono-magmatic evolution of Central Afar. *Tectonics* <http://dx.doi.org/10.1002/2015TC003893>.
- Stone, J.O., 2000. Air pressure and cosmogenic isotope production. *J. Geophys. Res. Solid Earth* 105, 23753–23759.
- Trull, T.W., Kurz, M.D., Jenkins, W.J., 1991. Diffusion of cosmogenic ^3He in olivine and quartz - implications for surface exposure dating. *Earth Planet. Sci. Lett.* 103, 241–256.
- Trull, T.W., Brown, E.T., Marty, B., Raisbeck, G.M., Yiou, F., 1995. Cosmogenic ^{10}Be and ^3He accumulation in Pleistocene beach terraces in Death-Valley, California, USA - implications for cosmic-ray exposure dating of young surfaces in hot climates. *Chem. Geol.* 119, 191–207.
- von Blanckenburg, F., 2005. The control mechanisms of erosion and weathering at basin scale from cosmogenic nuclides in river sediment. *Earth Planet. Sci. Lett.* 237, 462–479.
- Williams, A.J., Stuart, F.M., Day, S.J., Phillips, W.M., 2005. Using pyroxene microphenocrysts to determine cosmogenic ^3He concentrations in old volcanic rocks: an example of landscape development in central Gran Canaria. *Quat. Sci. Rev.* 24, 211–222.
- Yokochi, R., Marty, B., Pik, R., Burnard, P., 2005. High $^3\text{He}/^4\text{He}$ ratios in peridotite xenoliths from SW Japan revisited: evidence for cosmogenic ^3He released by vacuum crushing. *Geochim. Geophys. Geosyst.* 6. <http://dx.doi.org/10.1029/2004GC000836>.
- Zimmermann, L., Blard, P.H., Burnard, P.G., Medynski, S., Pik, R., Puchol, N., 2012. A new single vacuum furnace design for cosmogenic ^3He dating. *Geostand. Geoanal. Res.* <http://dx.doi.org/10.1111/j.1751-908X.2011.00145.x>.